Journal of the Korean Physical Society (2023) 83:65–71
https://doi.org/10.1007/s40042-023-00862-2

Online ISSN 1976-8524
Print ISSN 0374-4884

ORIGINAL PAPER - CONDENSED MATTER

Identification of octahedral configuration in strained $SrRuO_3$ thin films

Tae Hwa Eom[1] · Sang A. Lee[1] · Jae-Yeol Hwang[1]

Received: 19 May 2023 / Revised: 22 May 2023 / Accepted: 30 May 2023 / Published online: 19 June 2023

Abstract
The compressively strained (2 2 0)-oriented $SrRuO_3$ epitaxial thin films were grown on *c*-plane $SrTiO_3$ substrates using pulsed laser deposition. Temperature-dependent lattice changes associated with structural phase transition were investigated through in-situ X-ray diffractions with varying temperature ranges from 25 to 650 °C under atmospheric conditions. Strong modulation of the in-plane lattices between the strained $SrRuO_3$ thin film and $SrTiO_3$ substrate was observed. The structural phase transition from pseudo-orthorhombic to the tetragonal structure was determined at around 285 °C and epitaxial strain was persistent during the structural phase transition in the fully strained $SrRuO_3/SrTiO_3$ heterostructured thin film. Crystal symmetry and the corresponding RuO_6 octahedral configurations were verified that the compressively strained $SrRuO_3$ thin film has pseudo-orthorhombic (monoclinic, $P2_1/m$, #11) structure with the BO_6 configuration of $a^+a^-c^-$ at 25 °C and tetragonal ($I4/mcm$, #140) with the octahedral tilt of $a^0a^0c^-$ above 285 °C through structural model calculations based on the diffraction data of 20 individual half-order peaks.

Keywords $SrRuO_3$ · Strained thin film · Octahedral configuration · BO_6 octahedron · Structural phase transition

1 Introduction

$SrRuO_3$ has long been the core of extensive research for the fundamental sciences and potential applications for electronic and spintronic device applications due to its exclusive properties as an itinerant ferromagnetic 4*d* transition metal oxide, catalyst, and oxide conductor with metallicity [1–3]. ABO_3 perovskites with transition metal at *B*-site have been known that the deformations of BO_6 octahedra by Jahn–Teller distortions are attributed to ferroelectricity, metal–insulator transitions, and magnetic properties [4]. Such interesting properties are originated from the fundamentals of strongly correlated *d* electrons attributing the entangled interactions between lattice, charge, orbital, and spin through corner-shared BO_6 networks [4–6]. Interestingly, $SrRuO_3$ and $CaRuO_3$ have the same orthorhombic perovskite structure, but they show different magnetic properties due to the difference in the degree of BO_6 octahedral distortion. For these reasons, in perovskite heterostructures, many approaches have been studied to control these interesting properties associated with the structural configurations of BO_6 octahedra through the varying thickness, oxygen vacancy engineering, cation substitutions, adjusting epitaxial strain, and interfacial coupling of the superlattice [1, 7–11]. It has been reported that the apparent changes in the crystal structure and physical properties induced by structural phase transition (SPT) in the ABO_3 perovskites, such as $SrTiO_3$ (STO), $KTaO_3$, $LaAlO_3$, and $CaTiO_3$ [12–15], are relevant to the distortions and rotations of the BO_6 octahedra accompanying local symmetry breaking. SPT is a common phenomenon accompanying the distinctive variations in crystal symmetry and space group as a function of pressure and temperature. It has been known that SPT in $SrRuO_3$ (SRO) bulk is occurred from orthorhombic (*Pbnm*, #62) to tetragonal ($I4/mcm$, #140) and tetragonal to cubic ($Pm\bar{3}m$, #221) structure with increasing temperature above 300 K [16]. In the epitaxial thin films, SPT depends on the generated strain type between the SRO thin film and substrate since epitaxial strain can cause structural deformation along with the change in the RuO_6 octahedral rotation [7, 17–19]. For instance, SRO thin film on (1 0 0) STO with compressive strain has an orthorhombic structure at room temperature but becomes tetragonal above 285 ℃ whereas the SRO thin films

✉ Sang A. Lee
sangalee@pknu.ac.kr

✉ Jae-Yeol Hwang
jyhwang@pknu.ac.kr

[1] Department of Physics, Pukyong National University, Busan 48513, Korea

maintain a cubic phase under biaxial tensile strain. However, in the perspective of crystallography, the configuration of BO_6 octahedron associated with SPT has seldom been discussed even though the octahedral structure is a subset of crystal structure governed by the framework of a unit cell, lattice strain, and crystal symmetry. In the fully strained SRO thin films, the in-plane and out-of-plane interatomic distances are considerably dissimilar, resulting in variation in the overlap of Ru t_{2g} and O 2*p* orbitals in the two directions. Furthermore, the strain-induced deformations and the distortions of the RuO_6 octahedral networks strongly correlated to the *B*-O bond lengths and the *B*-O-*B* bond angles are vital to determine the physical properties since the electronic and magnetic properties are known to be associated with the degree of hybridization of Ru 4*d* and O 2*p* orbitals [20, 21]. Thus, for further advances to enhance the physical properties of SRO thin films based on structural engineering, the identification of BO_6 octahedral structure with crystal symmetry is crucial for the strategy for tailoring the electronic and magnetic properties in strained SRO thin films.

In this paper, we demonstrate the fully strained SRO thin films grown on STO substrates by pulsed laser deposition (PLD) to investigate the structural fundamentals, including crystal symmetry and BO_6 octahedral configuration. To elucidate the structural correlations between SRO thin film and STO substrate attributing epitaxial strain, the changes in lattice parameters, crystal symmetry, and octahedral structure are analyzed through in-situ X-ray diffractions with varying temperature ranges from room temperature to 650 °C by inducing SPT. In particular, the BO_6 octahedral configurations with the corresponding crystal symmetry and space group in the epitaxially strained SRO/STO heterostructures are identified by the structural model calculations based on the diffraction data of half-order peaks (HOPs).

2 Experiments and discussion

High-quality SRO thin films were grown on atomically TiO_2-terminated STO (0 0 1) single crystalline substrates using PLD. KrF excimer laser ($\lambda = 248$ nm; Coherent Inc., COMPex 205F, Coherent) with a fluence of 1.2 J/cm^2 and a repetition rate of 5 Hz were used. The distance between the SRO target and the STO substrate was fixed at 34 mm. The substrate temperature was maintained at 1023 K with oxygen partial pressure ($P(O_2)$) of 1×10^{-1} Torr during the film growth. The crystal structure, symmetry, epitaxy, and thickness of the SRO thin film were characterized by 9 kW high-resolution 6-circle X-ray diffractometer (HR-XRD, Rigaku SmartLab II, Rigaku) using the parallel beam mode with the monochromatized Cu $K\alpha_1$ radiation ($\lambda = 1.540592$ Å) and 2D-detector (Hypix-3000, Rigaku). Temperature-dependent structural evolutions associated with SPT were characterized by introducing Anton Paar DHS-1100 domed hot stage under atmospheric conditions. The temperature of the domed hot stage was finely controlled from 25 to 650 °C by a programmable temperature controller after attaching the samples to the stage with a covering graphite hemisphere shell. The thickness of the SRO thin film was characterized by X-ray reflectometry (XRR). The structural phase, crystal orientations, and the epitaxy relation of SRO thin films were characterized using XRD gonio-scan, φ-scan, and reciprocal space map with a 2D detector (2D-RSM). The interplanar distances and angles were extracted from the optimized diffraction conditions for the symmetric and asymmetric φ-scans and reciprocal space map (RSM) through numerical analysis based on the least-square fitting and iterative regression methods. Structural information and octahedral configurations were extracted by the calculations of a structural model made with Python code and the measured data of HOPs.

In Fig. 1a, the X-ray diffraction pattern of SRO thin film grown on STO substrate by PLD shows the pure orthorhombic structure without any secondary phase. The thickness of the SRO film was fixed at 16 nm, confirmed by XRR and the calculation from the thickness fringes. Also, the SRO thin film exhibits the Pendellösung fringes around (1 1 0) and (2 2 0) Bragg diffraction peaks, indicating the atomically smooth surface and a sharp heterointerface between the thin film and the underlying substrate. Structurally, in-plane lattices of SRO can be epitaxially aligned on that of STO substrate coherently because both have an ABO_3 perovskite structure with the same *A*-site Sr element and the corner-shared BO_6 octahedral networks. As such, cube-on-cube epitaxy can be favorably made as illustrated in Fig. 1b. Indeed, four-fold symmetric peaks, equally spaced by 90°, were observed in the φ-scans of 4 4 2 and 2 0 2 reflections for SRO thin film and STO substrate azimuthally (Fig. 1b). It is worth noting that two sets of four-fold symmetric peaks are observed at the same φ–angles. This implies that the SRO thin film was epitaxially grown by matching in-plane lattices of STO substrate satisfying the epitaxy relations of SRO $(1\ 1\ 0)_O \parallel (0\ 0\ 1)_{PC} \parallel$ STO (0 0 1) and SRO $(0\ 0\ 1)_O \parallel (1\ 0\ 0)_{PC}$ $[0\ 1\ 0]_{PC} \parallel$ STO (1 0 0) [0 1 0], where the subscript O and PC denote orthorhombic and pseudocubic, respectively. In general, when the SRO thin film is grown coherently on a substrate, the structure of the thin film is determined by the biaxial stress [22]. In the case of lower compressed lattice mismatch, the SRO thin film on the STO substrate has an orthorhombic structure. The RSM for the pseudocubic 1 0 3 reflection of the SRO thin film signifies that the SRO thin film is fully strained, indicating the lattice mismatch between SRO thin film and the STO substrate is 0.45% (Fig. 1c) [23]. Under compressive stress, the orthorhombic unit cell ($a_O \neq b_O \neq c_O$, $\alpha_O = \beta_O = \gamma_O = 90°$) of the SRO is distorted ($\gamma_O < 90°$), which can be described as

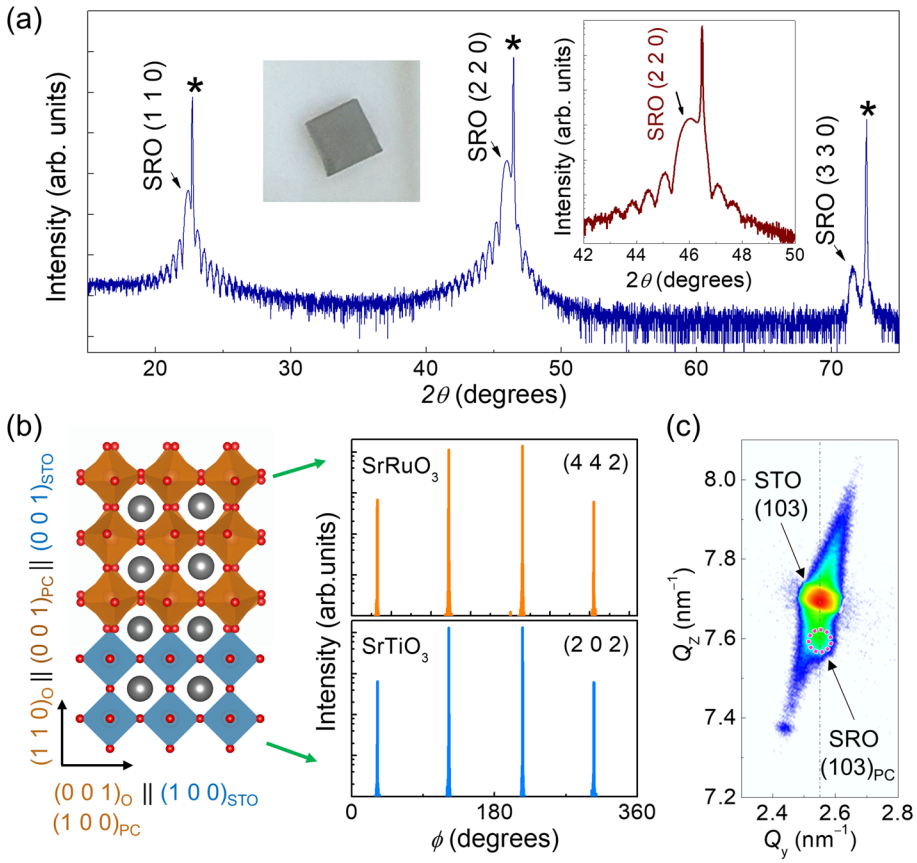

Fig. 1 Structural characterizations of the pristine $SrRuO_3$ thin films grown on $SrTiO_3$ substrates by pulsed laser deposition. **a** XRD θ–2θ scan of $SrRuO_3$ thin film. The insets show the magnified diffraction pattern for $SrRuO_3$ (2 2 0) diffraction peak in the photograph of the sample. **b** Schematics of $SrRuO_3/SrTiO_3$ heterostructure and the corresponding in-plane ϕ-scans. **c** Reciprocal space map for the pseudocubic 1 0 3 reflection of $SrRuO_3$ thin film. Asterisk (*) indicates substrate peak and the subscripts of O, PC, and STO denote octahedral, pseudocubic, and $SrTiO_3$, respectively

a pseudo-orthorhombic (or monoclinic) unit cell. As shown in Fig. 1b, the pseudo-orthorhombic SRO thin film can be considered as a pseudocubic hetero-structured thin film on the cubic STO substrate.

Figure 2 shows the experimentally characterized lattice parameter of the pseudocubic c_{PC} of the epitaxial SRO thin film from $(0\ 0\ 2)_{PC}$ peak and that of c_{STO} from STO (0 0 2) peak as a function of temperature. The lattice parameter values extracted from the XRD gonio-scans using Bragg–Brentano geometry show that SPT is occurred at around 285 °C (T_{SPT}, 558 K), well matched with others [19]. The calculated orthorhombic lattice parameters a_O and b_O of the SRO thin films during SPT were also shown in Fig. 2. The orthorhombic lattice parameters of a_o and b_o were determined from the off-axis SRO $(1\ 0\ 3)_{PC}$ diffractions for $\varphi = 0°$, 90°, 180°, and 270° during the temperature-dependent experiments. From the sudden change in the orthorhombic lattice parameters of a_O and b_O into the tetragonal lattices of a_T and b_T, the SPT from orthorhombic ($a_O \neq b_O$) to tetragonal ($a_T = b_T$) structure was clearly identified [24]. Interestingly, the T_{SPT} of the pseudocubic unit cell is lower compared to the T_{SPT} of the orthorhombic unit cell. The SPT in perovskite material is introduced in the RuO_6 octahedra framework. Therefore, the RuO_6 octahedra rotation, strongly constrained by the strain, is the result of a delayed response since our sample has a thin thickness [17]. The orthorhombic SRO in bulk system undergoes a structural phase transition, such as tetragonal to cubic structure, according to increasing temperature. In a thin film system, it is not easy to distinguish whether the crystal structure of the SRO thin films is tetragonal or cubic above T_{SPT}. The epitaxial SRO thin film is a tetragonally strained cubic (or pseudocubic) rather than a perfectly cubic structure since it is fully strained [17, 19]. STO substrate has a simple cubic structure without any TiO_6 octahedral distortion above room temperature except structural phase transition temperature of 110 K [25]. In addition, by comparing a_{PC} and c_{PC} before and after SPT at 300 K, we confirmed that the in-plane lattice parameters of the fully strained SRO thin film did not change and crystal symmetry was preserved after undergoing SPT. This result indicates that the epitaxial strain of SRO thin film is persistent during SPT [8]. In Fig. 3, gonio-scans for the off-axis diffractions around STO 2 0 4 reflections with the ϕ angles of 0, 90, 180, and 270°, corresponding to (4 4 -4), (2 6 0), (4 4 4), and (6 2 0) diffractions of rhombohedral SRO, shows that the as-grown SRO thin film has an orthorhombic structure ($a_O \neq b_O \neq c_O$) at room temperature. However, when SRO thin film is heated up to 300 °C, above T_{SPT}, the crystal structure of the SRO thin film is transformed into a tetragonal phase. This was verified by comparing four individual asymmetric $(1\ 0\ 3)_{PC}$

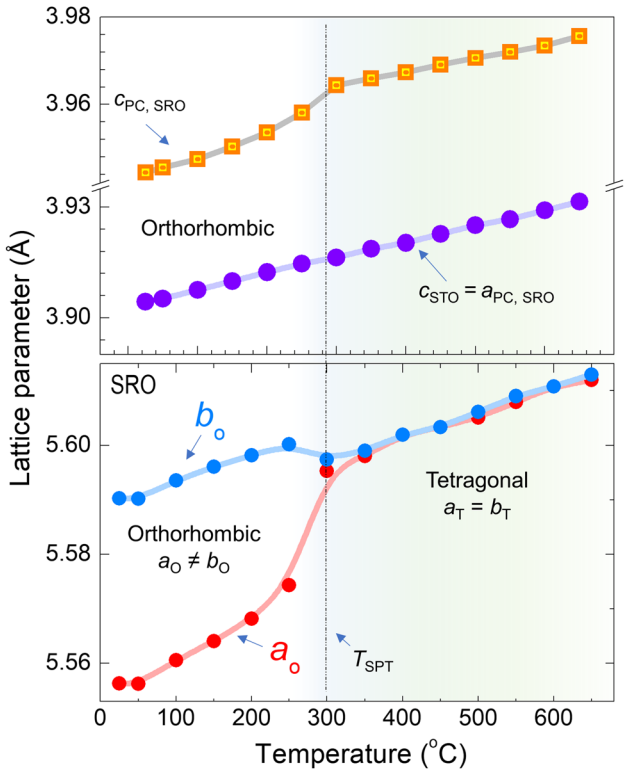

Fig. 2 The variations in the lattice parameters as a function of temperature acquired by temperature-dependent XRD for $SrRuO_3$ (SRO) thin film and $SrTiO_3$ substrate. Structural phase transition (SPT) of the SRO thin film from orthorhombic to tetragonal phase associated with the sudden changes in lattice parameters was identified at around 300 °C. Subscripts PC, O, and T indicate pseudocubic, octahedral, and tetragonal, respectively

diffractions acquired at the fixed ϕ-angles of 0, 90, 180, and 270°. Indeed, $(1\ 0\ 3)_{PC}$ diffraction peaks were consistently observed with similar intensity at 76° in 2θ regardless of the variations of ϕ-angles proving that the in-plane lattices are equal ($a_T = b_T$) with the uniform distributions of azimuthal domains.

The HOPs were analyzed to verify the BO_6 octahedral rotation strongly correlated to the crystal symmetry. First, $2\times2\times2$ supercell was made with the pseudocubic SRO lattice parameters ($a_{PC} = b_{PC} = 3.905$ Å, $c_{PC} = 3.944$ Å) to find the reciprocal positions of the measurable HOPs. Second, the diffractions of HOPs were characterized through HR-XRD. Finally, the qualitative information about the BO_6 octahedral rotations was determined based on model calculations. As shown in Fig. 4a, the HOP of the SRO (1/2 1/2/ 3/2), relevant to a^- rotation, can be not only utilized to identify the octahedral rotation along a_{PC} axis but also used as a barometer of SPT. According to the Glazer notation, 23 tilt systems of BO_6 octahedra are possible in ABO_3 perovskites [26]. Three distinguishable types of in-phase, antiphase (out-of-phase), and no rotations of the BO_6 octahedron are denoted by the superscript of +, –, and 0, respectively. The degree of BO_6 rotation is determined by a set of a, b, and c, which refer to the axes in the order $[100]_{PC}$, $[010]_{PC}$, and $[001]_{PC}$. Considering that the in-plane lattices of the fully strained SRO thin film are virtually equal to those of STO ($a_{PC} = b_{PC} < c_{PC}$) substrate and the pseudocubic axes are not orthogonal to each other ($\alpha_c \neq 90°$), $a^+a^-c^-$ corresponding to the space group of $P2_1/m$ satisfies all these conditions. This denotes that the crystal structure of the compressively strained SRO thin film is pseudo-orthorhombic (monoclinic, $P2_1/m$, #11) in contrast to the conventional crystal symmetry of SRO bulk (orthorhombic, *Pbnm*, #62) since any two—tilts means that the relevant pseudocubic cell axes are inclined to each other. Figure 4b and c show HOPs measured for $[1\ 0\ 0]_{PC}$ and $[0\ 0\ 1]_{PC}$ in the SRO thin film. In principle, the magnitude of HOP intensity is proportional to the degree of octahedral rotation along the corresponding axis. (1/2 1/2 3/2) diffraction relates to a^- rotation, disappeared with increasing temperature above T_{SPT} by SPT, proving the transformation of BO_6 octahedral configurations from $a^+a^-c^-$ to $a^0a^0c^-$. Accordingly, no diffraction of (1/2 1/2 3/2) was observed after SPT since a^- rotation was transformed into a^0, whereas (1/2 3/2 5/2) diffraction relevant to c^- was maintained but the degree of c^- rotation was diminished. Above T_{SPT}, if the fully strained SRO thin film on the STO substrate is cubic ($Pm\bar{3}m$) with $a^0a^0a^0$ rather than tetragonal ($I4/mcm$) with $a^0a^0c^-$, any out-of-phase octahedral rotation (–) should not be observed due to the absence of such BO_6 rotation in a cubic structure. However, the octahedral rotation of c^- is observed in the strained SRO thin film at 450 °C. Thus, the crystal structure of the compressively strained SRO thin film above T_{SPT} is obviously confirmed as the strained tetragonal structure ($a_T = b_T \neq c_T$) with the BO_6 octahedral configuration of $a^0a^0c^-$. Experimentally, the peak intensities were derived from the integrated area of the diffraction peak, measured through various HOPs along the h, k, and l directions [27–29]. The calculated intensity of each HOP to acquire precise rotation angles and volumetric fractions of structural domains can be evaluated by

$$I = I_0 \frac{1}{\sin\eta} \frac{1}{\sin 2\Theta} \left(\sum_{j=1}^{4} D_j |F_{hkl}|^2 \right),$$

where the octahedral structure factor F_{hkl} for 24 oxygen atoms in a $2\times2\times2$ pseudocubic SRO supercell, D_j is the relative volume fraction of structural domains, I_0 is the incident light intensity. $\frac{1}{\sin\eta}$ is a correction for the beam footprint, and $\frac{1}{\sin 2\Theta}$ is the Lorentz polarization factor [28]. Based on this model, custom-made Python code was used to determine the structural parameters, including octahedral rotation

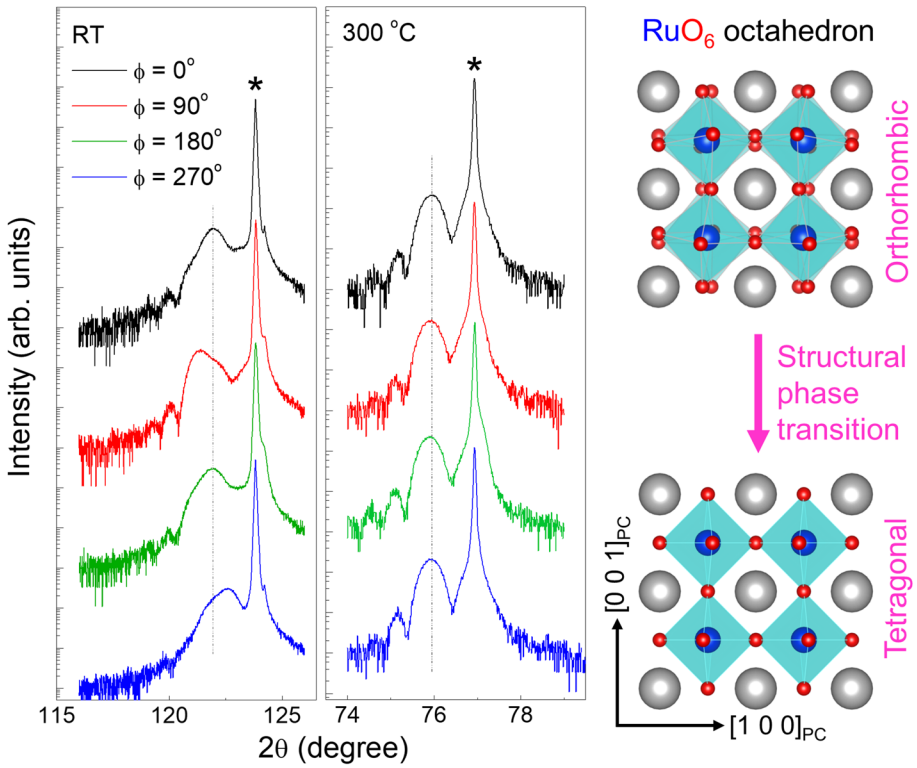

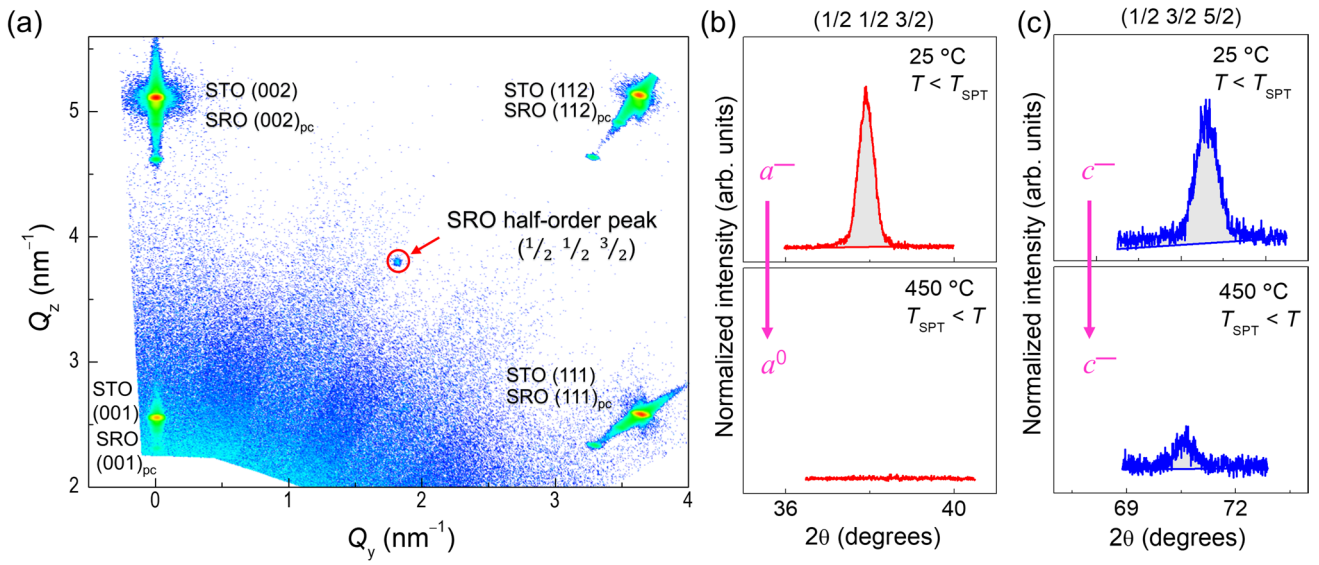

Fig. 3 Gonio-scans of the epitaxial $SrRuO_3$ thin films for (left) the asymmetric (4 4 − 4), (2 6 0), (4 4 4), and (6 2 0) diffractions at room temperature and (middle) the pseudocubic (1 0 3) diffractions at 300 °C with the ϕ-angle of 0, 90, 180, and 270 degrees, respectively. Asterisk (*) denotes the substrate peak. (right) the $(0\ 1\ 0)_{PC}$ views of $SrRuO_3$ for orthorhombic and tetragonal crystal structures with the corner-shared RuO_6 octahedral network

Fig. 4 **a** Wide range 2D reciprocal space map of $SrRuO_3/SrTiO_3$ heterostructured thin film and the measurable diffractions. The characterized half-order Bragg diffractions of **b** (1/2 1/2 3/2) and **c** (1/2 1/2 3/2) at 25 °C and 450 °C for $SrRuO_3$ thin film. RuO_6 octahedral rotation of $a-$ around $[1\ 0\ 0]_{PC}$ axis existed in pseudo-orthorhombic structure (at 25 °C) and vanished in tetragonal structure (at 450 °C) by structural phase transition

angles α, β, γ and four structural domain factors by minimizing the net difference between the measured and calculated diffraction intensities for HOPs through iterative regression methods using Nelder-Mead and sequential least squares programming algorithms.

As shown in Fig. 5, the crystal structures with the BO_6 octahedral configurations were visualized by the calculated structural factors from the diffraction data of 20 individual HOPs in the strained SRO thin films (Table 1). In the view of SRO $(0\ 1\ 0)_{PC}$, there is an obvious difference

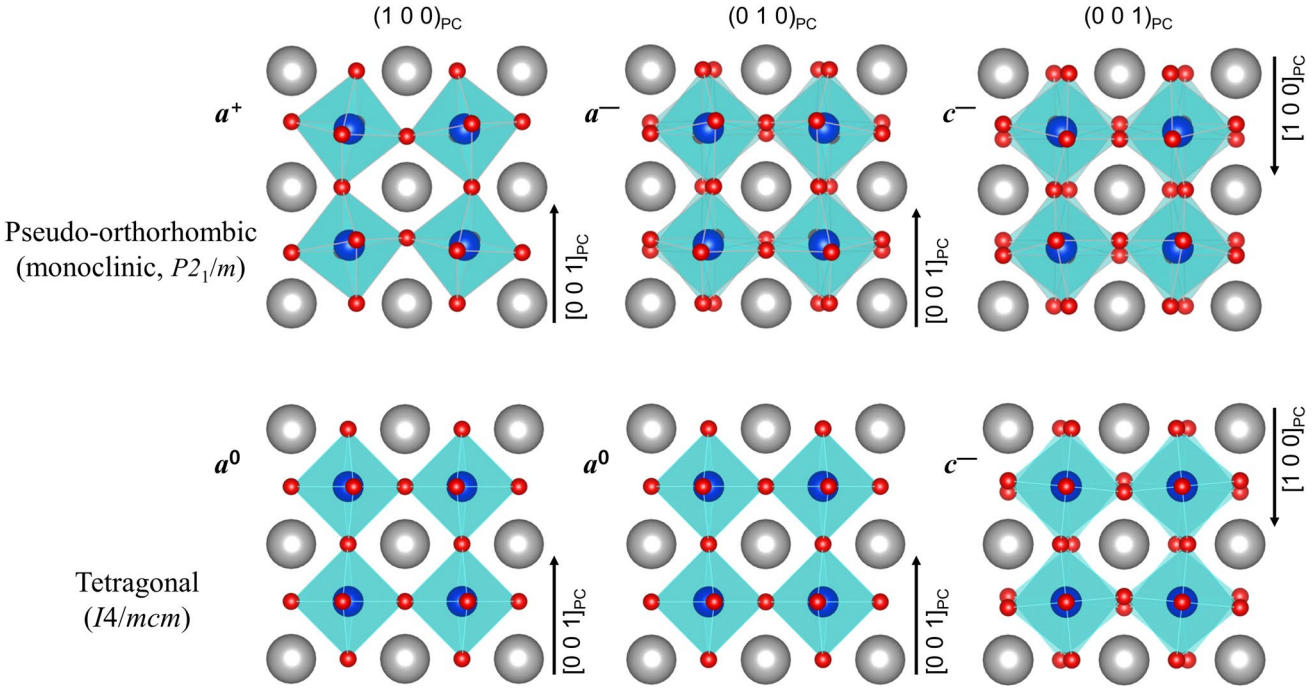

Fig. 5 The calculated BO_6 octahedral configurations of pseudo-orthorhombic and tetragonal structures with the corresponding tilts described by Glazer notation [26]

Table 1 The calculated structural factors from the X-ray diffraction data of half-order peaks in the strained $SrRuO_3$ thin films

$SrRuO_3$		Lattice parameters (Å)			Octahedral rotation (°)		
Temp.	Glazer notation.	*a*	*b*	*c*	*A*	*β*	*γ*
25 °C	$a^+a^-c^-$	3.905	3.905	3.944	5.2362	7.1962	7.2483
450 °C	$a^0a^0c^-$	3.922	3.922	3.969	0	0	2.4135

in BO_6 configurations of pseudo-orthorhombic (at 25 °C) and tetragonal (at 450 °C) structures, and the former shows antiphase a^- tilt whereas the latter has a^0 (no tilt) along $[0\ 1\ 0]_{PC}$ axis. Therefore, the octahedral configuration of the compressively strained SRO thin film was confirmed to be $a^+a^-c^-$ at RT ($300\ K < T < T_{SPT}$) and $a^0a^0c^-$ above T_{SPT} ($T_{SPT} < T < 923$ K) and the SPT from pseudo-orthorhombic (monoclinic) to tetragonal structure has occurred above 285 °C (558 K).

3 Conclusion

In summary, the compressively strained heteroepitaxial SRO thin films were coherently grown on the STO substrates using PLD. Temperature-dependent lattice changes and SPT were investigated through in-situ X-ray diffractions with varying temperature ranges from 25 to 650 °C. We verified that the in-plane lattices of the epitaxially strained SRO thin films were strongly modulated with those of STO substrate at varying temperatures. The SPT of the fully strained SRO thin film from pseudo-orthorhombic to the tetragonal system was identified at 285 °C (558 K) under atmospheric conditions. It was elucidated that the compressively strained SRO thin film has a pseudo-orthorhombic (monoclinic, $P2_1/m$, #11) structure with the BO_6 configuration of $a^+a^-c^-$ at 25 °C ($T < T_{SPT}$) and tetragonal ($I4/mcm$, #140) with the octahedral tilt of $a^0a^0c^-$ above T_{SPT} ($T_{SPT} < T$). This implies that the characterization of a half-order diffraction peak is a straightforward and powerful way to identify crystal symmetry, BO_6 configuration, and SPT at once in many perovskites. We suggest that there is a potential for harnessing octahedral configuration affecting electronic and magnetic properties in the perspective of interface and symmetry engineering as the epitaxial strain of SRO/STO heterostructure is persistent during SPT. Our finding provides a better understanding of the structural fundamentals of the BO_6 octahedral configurations correlated with epitaxial strain and SPT in ABO_3 perovskite materials for electronic and spintronic device applications.

Acknowledgements This work was supported by Pukyong National University Research Fund in 2019 (CD20191037) and the National Research Foundation of Korea (NRF) grant funded by the Korea government (MSIT) (NRF-2020R1F1A1073076). This research was supported by Basic Science Research Program through the National Research Foundation of Korea (NRF) funded by the Ministry of Education (NRF-2022R1I1A1A01065234).

Declarations

Conflict of interest There is no conflict of interest.

References

1. S.A. Lee et al., Enhanced electrocatalytic activity via phase transitions in strongly correlated $SrRuO_3$ thin films. Energ. Environ. Sci. **10**(4), 924–930 (2017). https://doi.org/10.1039/C7EE00628D
2. Q. Qin et al., Emergence of topological hall effect in a $SrRuO_3$ single layer. Adv. Mater. **31**(8), 1807008 (2019). https://doi.org/10.1002/adma.201807008
3. Y.M. Kwak et al., Magnetoresistance of epitaxial $SrRuO_3$ thin films on a flexible $CoFe_2O_4$-buffered mica substrate. Curr. Appl. Phys. **34**, 71–75 (2022). https://doi.org/10.1016/j.cap.2021.12.005
4. J.M. Rondinelli, N.A. Spaldin, Structure and properties of functional oxide thin films: insights from electronic-structure calculations. Adv. Mater. **23**(30), 3363–3381 (2011). https://doi.org/10.1002/adma.201101152
5. H.Y. Hwang et al., Emergent phenomena at oxide interfaces. Nat. Mater. **11**(2), 103–113 (2012). https://doi.org/10.1038/nmat3223
6. S.G. Jeong et al., Atomic and electronic structures of correlated $SrRuO_3/SrTiO_3$ superlattices. J. Korean Phys. Soc. **82**, 386–391 (2023). https://doi.org/10.1007/s40042-022-00695-5
7. D. Kan, R. Aso, H. Kurata, Y. Shimakawa, Thickness-dependent structure-property relationships in strained (110) $SrRuO_3$ thin films. Adv. Funct. Mater. **23**(9), 1129–1136 (2013). https://doi.org/10.1002/adfm.201202402
8. W.L. Lu et al., Control of oxygen octahedral rotations and physical properties in $SrRuO_3$ films. Phys. Rev. B **88**(21), 214115 (2013). https://doi.org/10.1103/PhysRevB.88.214115
9. B. Dabrowski et al., Reduced ferromagnetic transition temperatures in $SrRu_{1-v}O_3$ perovskites from Ru-site vacancies. Phys. Rev. B **70**(1), 014423 (2004). https://doi.org/10.1103/PhysRevB.70.014423
10. M.R. James, J.M. Steven, W.F. John, Control of octahedral connectivity in perovskite oxide heterostructures: an emerging route to multifunctional materials discovery. MRS Bull. **37**, 261 (2012). https://doi.org/10.1557/mrs.2012.49
11. S.A. Lee et al., Tuning electromagnetic properties of $SrRuO_3$ epitaxial thin films via atomic control of cation vacancies. Sci. Rep. **7**(1), 11583 (2017). https://doi.org/10.1038/s41598-017-11856-z
12. K.A. Müller, W. Berlinger, F. Waldner, Characteristic structural phase transition in perovskite-type compounds. Phys. Rev. Lett. **21**(12), 814–817 (1968). https://doi.org/10.1103/PhysRevLett.21.814
13. E. Pytte, J. Feder, Theory of a structural phase transition in perovskite-type crystals. Phys. Rev. **187**(3), 1077–1088 (1969). https://doi.org/10.1103/PhysRev.187.1077
14. S.A.T. Redfern, High-temperature structural phase transitions in perovskite. J. Phys. Condens. Matter **8**(43), 8267–8275 (1996). https://doi.org/10.1088/0953-8984/8/43/019
15. G. Shirane, Neutron scattering studies of structural phase transitions at Brookhaven. Rev. Mod. Phys. **46**(3), 437–449 (1974). https://doi.org/10.1103/RevModPhys.46.437
16. B.J. Kennedy, B.A. Hunter, High-temperature phases of $SrRuO_3$. Phys. Rev. B **58**(2), 653 (1998). https://doi.org/10.1103/PhysRevB.58.653
17. D. Kan, Y. Shimakawa, Strain effect on structural transition in $SrRuO_3$ epitaxial thin films. Cryst. Growth Des. **11**(12), 5483–5487 (2011). https://doi.org/10.1021/cg201070n
18. R. Aso, D. Kan, Y. Shimakawa, H. Kurata, Control of structural distortions in transition-metal oxide films through oxygen displacement at the heterointerface. Adv. Funct. Mater. **24**(33), 5177–5184 (2014). https://doi.org/10.1002/adfm.201303521
19. K.J. Choi et al., Phase-transition temperatures of strained single-crystal $SrRuO_3$ thin films. Adv. Mater. **22**(6), 759–762 (2010). https://doi.org/10.1002/adma.200902355
20. S. Tyagi et al., Strain healing of spin–orbit coupling: a cause for enhanced magnetic moment in epitaxial $SrRuO_3$ thin films. J. Phys. Condens. Matter **32**(30), 305501 (2020). https://doi.org/10.1088/1361-648X/ab8424
21. S.H. Chang et al., Thickness-dependent structural phase transition of strained $SrRuO_3$ ultrathin films: the role of octahedral tilt. Phys. Rev. B **84**(10), 104101 (2011). https://doi.org/10.1103/PhysRevB.84.104101
22. F. Spaepen, Interfaces and stresses in thin films. Acta Mater. **48**(1), 31–42 (2000). https://doi.org/10.1016/S1359-6454(99)00286-4
23. A. Vailionis, W. Siemons, G. Koster, Strain-induced single-domain growth of epitaxial $SrRuO_3$ layers on $SrTiO_3$: a high-temperature x-ray diffraction study. Appl. Phys. Lett. **91**(7), 071907 (2007). https://doi.org/10.1063/1.2771087
24. A. Vailionis et al., Misfit strain accommodation in epitaxial ABO_3 perovskites: lattice rotations and lattice modulations. Phys. Rev. B **83**(6), 064101 (2011). https://doi.org/10.1103/PhysRevB.83.064101
25. D. de Ligny, P. Richet, High-temperature heat capacity and thermal expansion of $SrTiO_3$ and $SrZrO_3$ perovskites. Phys. Rev. B **53**(6), 3013–3022 (1996). https://doi.org/10.1103/PhysRevB.53.3013
26. A.M. Glazer, Simple ways of determining perovskite structures. Acta Cryst. A **31**, 756 (1975). https://doi.org/10.1107/S0567739475001635
27. C.L. Jia et al., Oxygen octahedron reconstruction in the $SrTiO_3$/$LaAlO_3$ heterointerfaces investigated using aberration-corrected ultrahigh-resolution transmission electron microscopy. Phys. Rev. B **79**(8), 081405 (2009). https://doi.org/10.1103/PhysRevB.79.081405
28. S.J. May et al., Quantifying octahedral rotations in strained perovskite oxide films. Phys. Rev. B **82**(1), 014110 (2010). https://doi.org/10.1103/PhysRevB.82.014110
29. M. Brahlek, A.K. Choquette, C.R. Smith, R. Engel-Herbert, S.J. May, Structural refinement of Pbnm-type perovskite films from analysis of half-order diffraction peaks. J. Appl. Phys. **121**(4), 045303 (2017). https://doi.org/10.1063/1.4974362